


ORIGINAL RESEARCH

Generalised model predictive controller design for A DC–DC non-inverting buck–boost converter optimised with a novel identification technique

Seyyed Morteza Ghamari¹  | Fatemeh Khavari¹ | Hasan Molaei¹ | Patrick Wheeler²¹Faculty of Electrical And Computer Engineering, Shahrood University of Technology- Semnan, Iran²Faculty of Engineering, Nottingham University**Correspondence**

Seyyed Morteza Ghamari, Faculty of Electrical And Computer Engineering, Shahrood University of Technology- Semnan.

Email: mortaza.ghamari@yahoo.com**Abstract**

An on-line generalised model predictive control (GMPC) strategy is designed and optimised with a novel identification procedure in the presence of different disturbances. The principle of MPC is utilising a discrete-time model of a system to reach the control variables with a prediction over these values, which is followed by computing a cost function for the control aims. Non-inverting buck–boost converter is a non-minimum phase system based on its boost mode, which makes a challenging condition for designing a stable controller. The proposed control technique described in this paper removes the requirement for a system mathematical model adopting a black-box identification method which can decrease the computational burden. Numerous harmful disturbances can affect a DC–DC converter; thus, the GMPC scheme is used along with a novel improved exponential regressive least identification algorithm as an adaptive strategy for the controller to optimise the gains of the controller in an on-line way resulting in better disturbance rejection. A PID controller with particle swarm optimisation algorithm is designed for this converter to be compared with the GMPC controller. Finally, the efficiency of the GMPC is verified in various performances with experimental and simulation results.

1 | INTRODUCTION

Nowadays, DC–DC power converters are playing an influential role in producing electrical power for industrial users. The main goal behind using power converters is the regulation of output voltage of a load and providing appropriate dynamic performance [1–4]. To fulfil this aim plenty of controllers have been designed for converters to enhance their operation [5, 6], limit switching losses [7], and increase efficiency [8, 9]. Based on some working characteristics of a power converter, controllers with a flexible and well-behaved dynamics are needed. The important concern about a converter is its good performance during disturbances which cannot be guaranteed by the control strategies with fixed compensation parameters. Meanwhile, a popularity is growing for the control techniques containing more well-behaved structures, which has led to the digital controllers in switching circuits. Because of the switching properties of buck–boost converters and the non-minimum structure

presented by boost typologies, methods such as sliding-mode [10], dead beat [11], and internal model controllers [12, 13] are proposed which using an adaptive mechanism. The primary pros of dead beat, internal model, and sliding-mode structures is providing output voltage without overshoot and ringing. Meanwhile, the complexity of dead beat and internal model control schemes makes them unpopular alternatives [14, 15]. For example, sliding-mode technique behaves better in transients, parametric alterations, and chattering issues.

The fundamental theory behind model predictive control (MPC) built with a horizon method which calculates control signals with an optimising process for a future time step. One of the major issues for power converters is their stability and MPC is a promising technique since it is fundamentally robust enough of systematically compensating non-linearity of system, state and input constraints along with ensuring optimally considering the cost functions. However, these benefits suffer from a large computational burden in the controller. In refs.

This is an open access article under the terms of the [Creative Commons Attribution](https://creativecommons.org/licenses/by/4.0/) License, which permits use, distribution and reproduction in any medium, provided the original work is properly cited.

© 2022 The Authors. *IET Power Electronics* published by John Wiley & Sons Ltd on behalf of The Institution of Engineering and Technology.

[16–18], a general review is reported based on MPC for switching power converters. Furthermore, two types of MPC strategies are illustrated as continuous control set MPC (Ccs-MPC) and finite control set MPC (Fcs-MPC) approaches. It is presented that in Fcs-MPC, the cost function and system states are predicted regarding the switching conditions which is driven for the following period. Fcs-MPC yields fast and robust closed-loop dynamics; yet, is limited in prediction horizon based on the significant growth of prediction horizon length with the switching combinations in the range of one or two prediction steps [19–22]. In most cases of Ccs-MPC, pulse width modulation (PWM) technique is utilised in generating control signal based on the duty cycle [23, 24]. An online optimisation of the system is the major concern of this strategy which is handled offline by explicit model predictive control (EMPC) [25–28]. EMPC produces some feedback control laws along with tree searches to reach the state feed-back laws which needs a large storing capacity and short prediction horizons. Different approaches are presented to tackle the online optimisation issue with a fast calculation time and better prediction horizons [29–31]. These papers provide on-line optimisation strategies of MPC for different converters with less calculation time and a prediction horizon of around 400 to 600 μ s. Despite the better results presented by these papers in comparison with FCS-MPC or E-MPC alternatives, they are not completely satisfying. To provide less complex structures model free methods, which can use system identification to get the system dynamic without knowing the actual dynamic, are introduced. In refs. [32–34], an ANN-based control is proposed for different applications such as power converters. In these approaches, since the whole system is a black-box, the requirement for the mathematical model is removed and the performance of the controller is optimised by a better parametric tuning. However, the main drawback of this type of methodology is their dependence on a wide range of training data. In refs. [35–37], a robust self-tuning adaptive controller is designed with a novel identification technique for power converters using black-box scheme with a great convergence and a robust dynamics in disturbances. The estimation method was improved in these works to provide better parametric tuning; yet, the robustness of the controller is focused on the estimator. This paper describes an online optimised MPC strategy with a novel improved exponential regressive least-square (IERLS) identification technique providing a low computational burden and more prediction horizons. Contributions provided by this method are:

- An advance control method is designed, which has reached a good performance with an excellent stability without the mathematical model of the converter and without a predefined cost function to be minimised at each sampling time (T_s) that is called end-to-end technique.
- Fast dynamic performance, less computational cost, and improved steady-space performance are provided.
- The prediction horizons are increased presenting accurate trajectory tracking control.
- Challenging constrains are discussed on the system, which are solved by the controller.

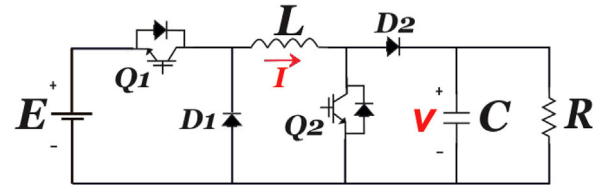


FIGURE 1 Non-inverting buck–boost converter

- Significant adaptation of MPC to model parameters variations with better parametric estimation is proposed for system identification.

2 | DC-DC NON-INVERTING BUCK-BOOST CONVERTER MODELLING

Buck–boost converter is classified in the class of attenuation or chopper circuits (Figure 1). This topology is built by different components as follows: capacitor C, inductor L, resistor R (load), and voltage source E as well as diodes (T_2 and T_1) and switches (Q_2 and Q_1).

Transistor-diode symbols are used to form circuit schematic of the converter in Figure 1. Also, two operational modes are introduced based on u that is the switching function. Two different modes are classified by this topology for buck and boost mode. Overall, to present buck functional state, the controller must operate such that the level of the output voltage on the load be lower than supply voltage. Consequently, to satisfy this condition, Q_1 switch will be fired while Q_2 is off. However, when the higher output voltage is produced compared to input voltage, the converter works in boost mode (Q_2 starts to fire when Q_1 stays constantly on). Linearising the state-space averaging model around the operating point is used to get the system's small signal transfer function. The transfer functions for buck and boost modes are driven based on output voltage (\hat{V}_C) and control input (\hat{d}) in Equations (1) and (2) [38].

$$\hat{V}_C = \frac{\frac{E}{LC}}{s^2 + \frac{s}{RC} + \frac{1}{LC}} \hat{d} + \frac{\frac{D_1}{LC}}{s^2 + \frac{s}{RC} + \frac{1}{LC}} \hat{E} \quad (1)$$

$$\hat{V}_C = \frac{\frac{I_L}{C} \left(\frac{E}{LI_L} - s \right)}{s^2 + \frac{s}{RC} + \frac{(1-D_2)^2}{LC}} \hat{d} + \frac{\frac{(1-D_1)}{LC}}{s^2 + \frac{s}{RC} + \frac{(1-D_2)}{LC}} \hat{E} \quad (2)$$

where D_1 and D_2 show the duty cycles of switches. Also, the superscript “ $\hat{\cdot}$ ” illustrates a minimal AC variation around the steady-state operating point. Considering the transfer function of the converter, the impact of capacitor resistance (R_C) among the parasitic elements is the only effective factor providing a

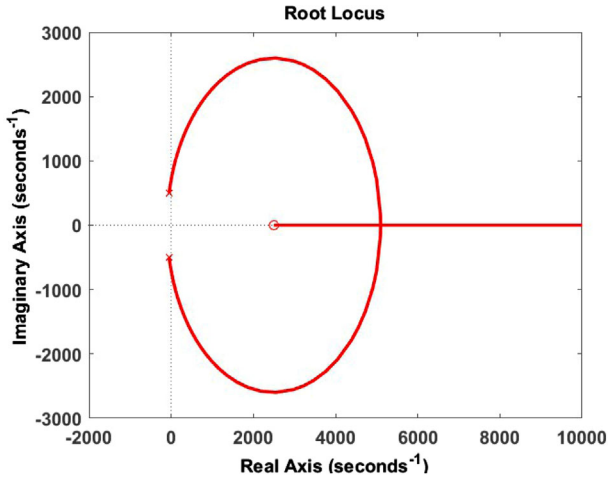


FIGURE 2 Pole and zero placement of the system

zero in the transfer function. It should be noted that the series diodes have a small range threshold voltage and it is possible to be ignored; also, the on-resistance of switches can be estimated about 0.8 ohm that can be ignored since it has a small amount. Thus, one can omit other parasitic elements from small-signal analysis of the circuit; however, their influence are applied in both experimental and simulation results. The relation between the capacitor voltage and the output voltage is shown in Equation (3).

$$\widehat{V}_o = (1 + R_C C_s) \widehat{V}_C \quad (3)$$

A combination of Equations (1)–(3) without considering the input voltage dynamics can calculate the transfer function of the control input (duty cycle) to the output voltage for both buck and boost modes as below:

$$\widehat{V}_o = \frac{\frac{E}{LC}(1 + R_C C_s)}{s^2 + \frac{s}{RC} + \frac{1}{LC}} \widehat{d} \quad (4)$$

$$\widehat{V}_o = \frac{\frac{I_L}{C} \left(\frac{E}{RC} - s \right) (1 + R_C C_s)}{s^2 + \frac{s}{RC} + \frac{(1 - D_2)^2}{LC}} \widehat{d} \quad (5)$$

It should be noted that the role of R_c can play a crucial impact on the ripple of output voltage and generates a ripple voltage. Also, the boost mode consists of a right half plane zero (RHPZ), which adjusts a hard constraint on the achievable performance and makes the system a non-minimum structure as depicted in Figure 2.

To function the digital GPC technique, digital discrete transfer function of the proposed system is needed, which zero-order hold drives this duty.

$$G(z) = \frac{Y(z)}{U(z)} = \frac{b_0 z + b_1}{z^2 + a_1 z + a_2 z} \quad (6)$$

Furthermore, to estimate b_1 , b_0 , a_2 , and a_1 parameters, an identification method is used that has been explained in more details in the following sections.

3 | RLS IDENTIFICATION PROCESS

RLS identification technique is a well-known estimator owing to its prominent benefits, namely: easy implementation, high efficiency in real-time operations, dynamical adaptability, and low memory capacity [39–41]. Equation (7) shows the cost function of RLS technique.

$$J = \frac{1}{N} \sum_{n=1}^N e^T(z) e(z)$$

$$e(z) = y(z) - \widehat{y}(z) \quad (7)$$

In Equation (7), $e(z)$ shows the error function where Equation (8) depicts the discrete digital transfer function.

$$y(z) = -a_1 y(z-1) + b_0 u(z-1) \quad (8)$$

Equation (8) can help to reach the Equation (9).

$$y(z) = \phi(z) \theta(z)$$

$$\phi(z) = [u(z-1), u(z-2), -y(z-2), -y(z-1)] \quad (9)$$

$$\theta(z) = [b_1, a_1, b_0, a_2]^T$$

Equation (9) shows two coefficients of ϕ and θ that are vectors depicts the gains of estimation and observation. However, the past data-driven of u and y can be held in the ϕ . Alternatively, this estimator tries to update the cost function repeatedly. Meanwhile, because the power converters are electrical devices working in different applications, it is possible that various disturbances can have a negative impact on their dynamics. Compensating these disturbing effects can be satisfied with an improvement over the identification algorithm.

Thus, to adopt this development, a factor called λ is applied to the RLS estimator capable of expanding the weighing function. To main benefits can be provided by this factor: the range of parametric estimation is widened, resulting in more accurate results and regular update of parametric estimation considering the latest alterations. Equation (10) illustrates this algorithm, so-called the “forgetting factor algorithm”.

$$\widehat{\theta}(z) = [\theta(z-1) \phi^T(z) - y(z)] K(z) + \widehat{\theta}(z-1)$$

$$K(z) = (\lambda I + \phi^T(z) P(k-1) \phi(z))^{-1} \phi(z) P(k-1) \quad (10)$$

$$P(z) = P(k-1) K(k) \phi^T(z) - P(k-1)$$

The extra factor of λ is called “time-varying forgetting factor”, which is defined by $\lambda = e^{\frac{-j}{T_f}}$. In this definition, T_f and j are time constant exponential forgetting and sampling cycle. Equation (10) shows two functional matrices of $P(z)$ and $K(z)$,

TABLE 1 Buck mode estimation results with RLS identification strategy

Parameter	Mathematical amounts	Real-time values
a_1	-1.049	-1.042
a_2	0.136	0.125
b_0	1.257	1.201
b_1	-1.168	-1.096

TABLE 2 Boost mode estimation results with RLS identification strategy

Parameter	Mathematical amounts	Real-time values
a_1	-1.049	-1.045
a_2	0.1375	0.125
b_0	0.838	0.789
b_1	-0.779	-0.609

while there are known as adaption matrix and covariance matrix. The following clarification is used to better describe the role of λ in Equation (11): if the term of $1 > \lambda$ is reached, the rate of $K(\mathcal{z})$ and $P(\mathcal{z})$ can be high. The primary benefit of this algorithm is the constant strength that occurred in tracking and compensating the variations that appeared in the system dynamics.

This developed algorithm with λ is called ‘‘Exponential RLS’’ algorithm or ERLS.

A range is introduced in Equation (11) to dedicate the rate of λ .

$$\lambda(t) = \min[\lambda(t-1)\lambda_0 + (-\lambda_0 + 1)], \quad 1 - \frac{\varepsilon^2}{\Sigma_0} \quad (11)$$

Assuming λ as the initial rate, the following procedure can be defined for Equation (11): assuming the system is in the steady-state condition, ε can be low or zero while, this can stimulate the λ to be one or excess it. On the other hand, the level of ε goes up when some disturbances appear in the system leading a significant drop over the λ . This process influences on the $K(\mathcal{z})$ and $P(\mathcal{z})$ matrices which is followed by an improvement on the parametric estimation of the identification method.

3.1 | Identification procedure

Tables 1 and 2 depict the estimated values in the mathematical and practical environments for both working modes.

It can be seen that there is a minimal difference between these values which can appeared based on the real-time disturbance such as components’ tolerance or aging. However, this distortion cannot make any difficulties for the control stage.

3.2 | Improved ERLS identification method

The term of λ , time variable feature, added to the RLS algorithm performs as a speed convergence adjuster in the dynamical per-

formances. However, if the value of λ is minimal, the parametric estimation can be fast; meanwhile, the negative impact of a significantly large disturbance on the system can increase consistently over the longer operations. The algorithm updated by λ is exponential RLS or ‘‘ERLS’’ method. Another issue associated with this technique is its poor performance in unactuated conditions. In this condition, the regressive matrix is zero and the following estimation relationships are reached:

$$\begin{aligned} P(t+1) &= \frac{1}{\lambda} P(t) \\ \theta(t+1) &= \theta(t) \end{aligned} \quad (12)$$

Equation (12) demonstrates that, the estimated values of θ with all eigenvalues of one and P matrix with all eigenvalues of $\frac{1}{\lambda}$, are unstable. Consequently, to clarify this condition, estimator ending situation, the following assumption is presented: first, estimation is constant; if $\lambda < 1$, P matrix will rise swiftly; also, a large variation will occur. Thus, to compensate these outcomes, a method is introduced known as conditional updating. Furthermore, in this new criterion the estimation regarding covariance matrices is being updated under actuation. Finally, the estimation procedure is enhanced by this factor that tries to update the pattern of covariance matrix under the occurrence of Equation (13), which can hinder this issue [42].

$$\phi(t)^T P(t) \phi(t) > 2(-\lambda + 1) \quad (13)$$

A novel method is used here to handle this issue which develops the covariance matrix that is ‘‘fixed matrix rejection method’’. Subsequently, applying this method needs bounding of the coefficients of covariance matrix resulting in robust performances over the ratios of estimator. In addition, exerting this technique in the estimator can hinder the exponential rise of covariance matrix when the regressive matrix is constant. Equation (14) depicts this new improved method.

$$\begin{aligned} \widehat{\theta}(\mathcal{z}) &= [y(\kappa) - \phi(\kappa)^T \theta(-1 + \mathcal{z})] K(\kappa) + \widehat{\theta}(-1 + \kappa) \\ K(\kappa) &= \phi(\mathcal{z}) P(-1 + \mathcal{z}) [\lambda I + \phi^T(\mathcal{z}) \phi(\mathcal{z}) P(-1 + \kappa)]^{-1} \\ \overline{P(\kappa)} &= \frac{1}{\lambda} [P(-1 + \kappa) - \left(\frac{\phi(\mathcal{z}) P(-1 + \kappa) \phi(\kappa)^T P(-1 + \kappa)}{I} \right. \\ &\quad \left. + \phi^T(\mathcal{z}) P(-1 + \kappa) \phi(\mathcal{z}) \right) \\ P(\kappa) &= c_1 \frac{\overline{P(\kappa)}}{\text{tr} P(\kappa)} + c_2 I \end{aligned} \quad (14)$$

An assumption of $c_1 > 0$ and $0 \leq c_2$ can be considered. The parameters are selected as Equation (15):

$$\begin{aligned} \frac{c_1}{c_2} &\approx 10^4 \\ \phi(\kappa)^T \phi(\kappa) c_1 &\gg 1 \end{aligned} \quad (15)$$

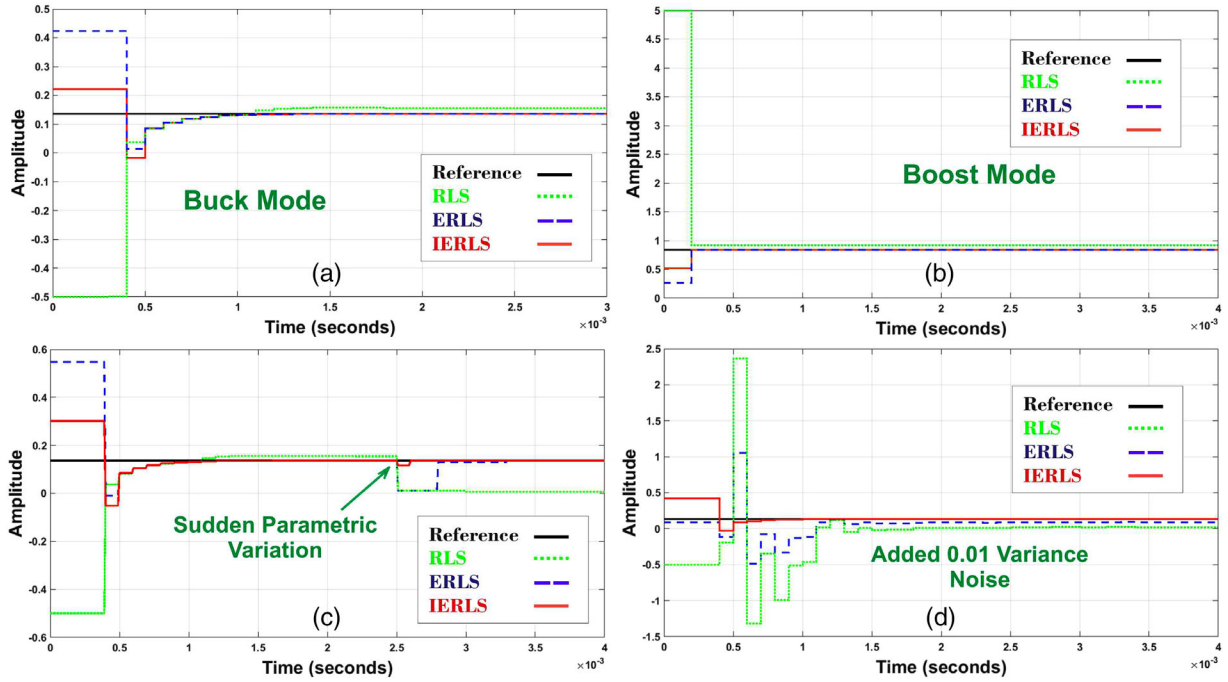


FIGURE 3 Comparison results between the presented identification procedures with a resistance load ($R = 10 \Omega$); (a) parametric estimation for the value of 0.136 in buck mode, (b) parametric estimation for the value of 0.835 in boost mode, (c) parametric estimation of the parameter with the value of 0.136 with sudden parametric variation, (d) parametric estimation of 0.835 with applied 0.01 variance noise

A general comparison is done in Figure 3 based on the performance of these identification techniques in different scenarios to observe their outcomes in challenging conditions.

In Figure 3, different operations are compiled to check the identification methods efficiency. By a glance look on Figure 3(a,b), it is vivid that a perfect convergence has reached by RLS, ERLS, and IERLS methods to the real parameters of 0.136 and 0.835 in buck and boost modes, but a minimal difference can be seen for RLS estimation, that is not a serious matter. In Figure 3(c), the operation of these estimators have been evaluated under sudden parametric variations, while IERLS and ERLS strategies depict an excellent converging; however, RLS method does not have the potential in managing the negative impact of this deviation. Moreover, to check the influence of noise on the performance of the identification methods, a noise with 0.01 variance is applied in Figure 3(d), where RLS estimator is unable to get the proper value and ERLS technique is showing its effort to get the estimated parameters in longer terms that provides a hard condition for GMPC to generate the control signal; meanwhile, IERLS technique demonstrates robust dynamics in overcoming this disturbance, which proposes it as the most suitable option for challenging conditions.

4 | GENERALISED MODEL PREDICTIVE CONTROL

The GMPC method is a well-known MPC method since it contains a good performance with a great robustness for both

academia and industry [18]. The principle behind GMPC is based on calculating a signal sequence of future control, while the goal is to reach a minimum value of a multistage cost function depicted on a prediction horizon. In addition, the optimisation index is the expectation of a quadratic functions calculating the difference among the predicted reference and the predicted system outputs; also, this reference is obtained on the horizon, where the control effort is measured by a quadratic function [40, 43]. The general block diagram of GMPC is shown in Figure 4.

The single input single output (SISO) system is assumed as Equation (16).

$$y(t)A(z^{-1}) = u(t)B(z^{-1}) + C(z^{-1})e(t) \quad (16)$$

Here A , B , and C are system's polynomials, while $u(t)$ is input, $y(t)$ is output, and $e(t)$ is noise. Also, this function is controller auto-regressive moving-average (CARMA) model. Based on the points discussed in ref. [44], an integrated CARMA model is the most suitable alternative for many industrial applications with the presence of non-stationary disturbances. This model is as below

$$y(t)A(z^{-1}) = u(t)B(z^{-1}) + C(z^{-1})\frac{e(t)}{(\Delta)} \quad (17)$$

where $\Delta = 1 - z^{-1}$ and for white noise, the C is chosen as 1. The generalised predictive control strategy contains of applying

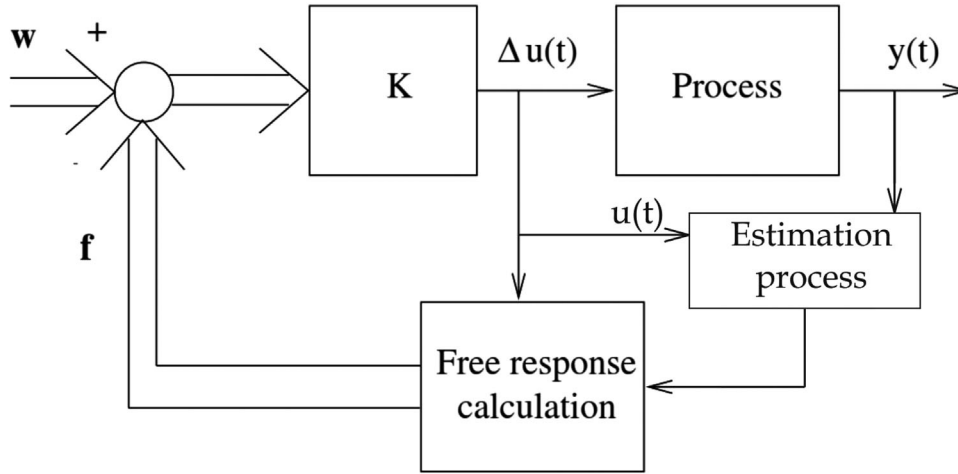


FIGURE 4 Block diagram of GMPC

a control sequence that minimises a multistage cost function of the form

$$J(N_2, N_1, N_u) = \sum_{j=N_1}^{N_u} \delta(j) [\hat{y}(t+j|t) - \omega(j+t)]^2 + \sum_{j=1}^{N_u} [\Delta u(j+t-1)]^2 \lambda(j) \quad (18)$$

In Equation (18), output system prediction over the optimum j step is shown as $\hat{y}(t+j|t)$, the control horizon is N_u , $\lambda(j)$, and $\delta(j)$ are weighting sequences, N_2 and N_1 are the maximum and minimum costing horizons, and $\omega(t+j)$ is the future reference trajectory. Computing the future control sequence, $u(t), u(t+1), \dots$, is the purpose of predictive control and must be done as the future plant output $y(t+j)$ gets close to $\omega(t+j)$, which is carried out by minimising $J(N_1, N_2, N_u)$. The optimal predictions of $j \geq N_1$ and $j \leq N_2$ are fundamental factors in optimising the cost function $y(t+j)$. Equation (19) is the diophantine equation:

$$1 = E_j(\bar{z}^{-1})\tilde{\Delta}A(\bar{z}^{-1}) + \bar{z}^{-1}F_j(\bar{z}^{-1}) \quad (19)$$

where $A(\bar{z}^{-1})\Delta = \tilde{A}(\bar{z}^{-1})$. The polynomials E_j and F_j are illustrated with degrees $j-1$ and na , respectively. We obtain them by dividing 1 by $\tilde{A}(\bar{z}^{-1})$ until the remainder can be factorised as $\bar{z}^{-1}F_j(\bar{z}^{-1})$. Therefore, $E_j(\bar{z}^{-1})$ and $F_j(\bar{z}^{-1})$ are illustrated as follows:

$$E_j(\bar{z}^{-1}) = e_{j,0} + e_{j,1}\bar{z}^{-1} + \dots + e_{j,j-1}\bar{z}^{-(j-1)} \\ F_j(\bar{z}^{-1}) = f_{j,0} + f_{j,1}\bar{z}^{-1} + \dots + f_{j,na}\bar{z}^{-na} \quad (20)$$

The best prediction of $y(t+j)$ is

$$y(t+j) = \Delta G_j(\bar{z}^{-1})U(j+t-1) + F_j(\bar{z}^{-1})y(t) \quad (21)$$

$U(t)$ represents future horizons of the input signal and the term of $G_j(\bar{z}^{-1})$ is shown as $E_j(\bar{z}^{-1})B(\bar{z}^{-1})$. However, sum of the past output term $F_j(\bar{z}^{-1})$ is called free response, f , and system response to future value is force response. One can reach to the optimal control signal by minimising Equation (22).

The best prediction of $y(t+j)$ is

$$\frac{\partial J}{\partial U} = 2(G^T G + \lambda I)U + 2G^T(f - w)\lambda \quad (22)$$

where $U = (w - f)(GG^T + \lambda I)^{-1}G^T$. In Equation (22), f represents the free response of the system, λ is the weighting factor and w is the reference trajectory. As noted before predictive controller uses prediction horizons to track the reference signal. To illustrate this process, four prediction horizons are shown for output and control signals in Figure 5(a,b).

It can be seen that as the prediction horizons of the controller increases, better output tracking signals will be generated for this structure which shows the need for model predictive controllers with higher number of horizons and less complex structures. The GMPC is able to completely satisfy these factors.

5 | PSO-PID CONTROLLER

This algorithm is an evolutionary computational method that is using swarm as research engine and an evolutionary operator [45]. Handling the d -variable operating problem in the d -dimensional search space requires a flock. Next, the best fitted position and speed will be selected considering the data achieved from the most suitable amounts. Figure 6 depicts PSO-based block diagram.

6 | SIMULATION RESULTS

Performance of the designed GMPC is verified using circuit parameters shown in Table 3. Firstly, the converging results

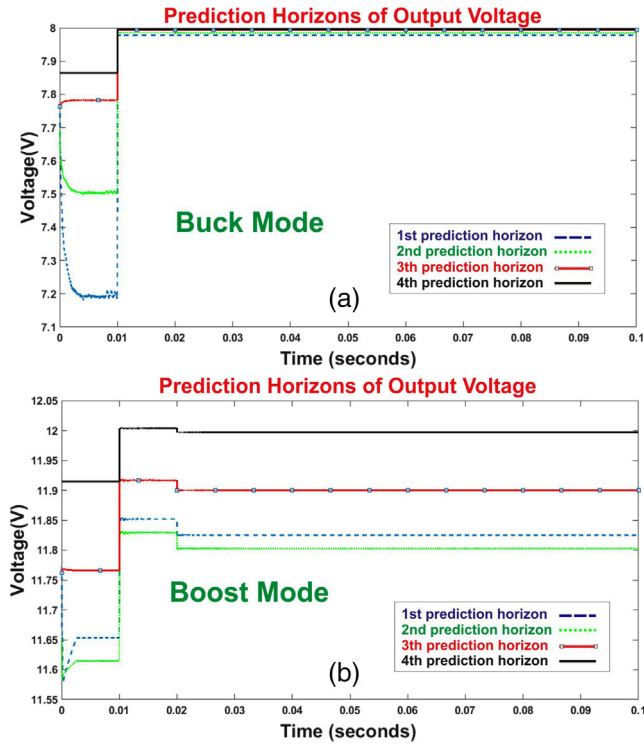


FIGURE 5 Operating modes of the converter for a resistance load with GMPC; (a) four prediction horizons of control signal in buck mode for the reference of 8 V, (b) four prediction horizons of output signal in boost mode for the reference of 12 V

of the GMPC and PSO-PID strategies are driven in Figure 7 without applying harmful disturbances.

Table 4 has analysed the performance of the controllers in Figure 7 to better clarify the superiority of GMPC over conventional method in both moods. Observing the comparison of Table 4, one can clearly understand the superiority of GMPC with the least amount of error and faster settling period. Additionally, the parameters of the PID method by proposed algorithms are listed in Table 5.

Different phenomena including aging or increasing temperature of components are able to alter the amounts of components resulting in the change of model parameters; thus, changing model parameters can divert the control method from

TABLE 3 Values of buck–boost converter parameter

Description	Parameters	Values
Supply voltage	E	10–20 V
Output voltage	V_{out}	5–30 V
Load resistance	R	10 Ω
Capacitor equivalent resistance	R_C	5 m Ω
Inductor equivalent resistance	R_L	2 m Ω
Diode resistance	R_{D1}, R_{D2}	40 m Ω
Switch resistance	R_{s1}, R_{s2}	3.7 m Ω
Inductor	L	10 μ H
Capacitor	C	1000 μ F
Diode threshold voltage	V_D	0.7 V

an ideal performance. Next, the operation of GMPC with IERLS scheme is tested in sudden load variations as parametric variation. A sudden parametric variation is stimulated in Figure 8 presenting the great response of GMPC under parametric variations.

It is an indisputable fact that in the real environments the level of reference voltage increases or decreases for the usage of output load. Thus, the proposed controller must be robust enough to track the reference alterations, which has been tested in Figure 9 for two negative and positive changes. First variation is a level of 12 to 8 V and the second one is 8 to 11 V that are significant variations for the control methods. Supporting the results shown in Figure 9, an analyse is done in Table 6 reaffirming the considerable strength of the GMPC under these problematic situations.

On the other hand, the impact of noise is an inevitable disturbance in industrial applications showing destructive impacts on the control performance. So, Figures 10 and 11 are depicting the effectiveness of the control strategies under the presence of noise with rates of 0.1 and 0.01 variances.

The noises that are applied in Figures 10 and 11 over the converter's structure can result in difficulties for the control methods. Clearly, the classical controller faces big deviations in its performance, while GMPC illustrates significant performances in handling the influence of noise introducing it as a prominent choice for practical applications.

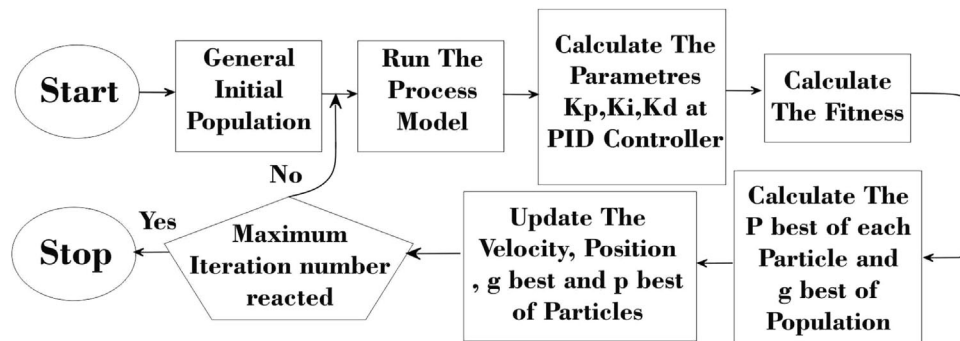


FIGURE 6 Flow chart of PSO

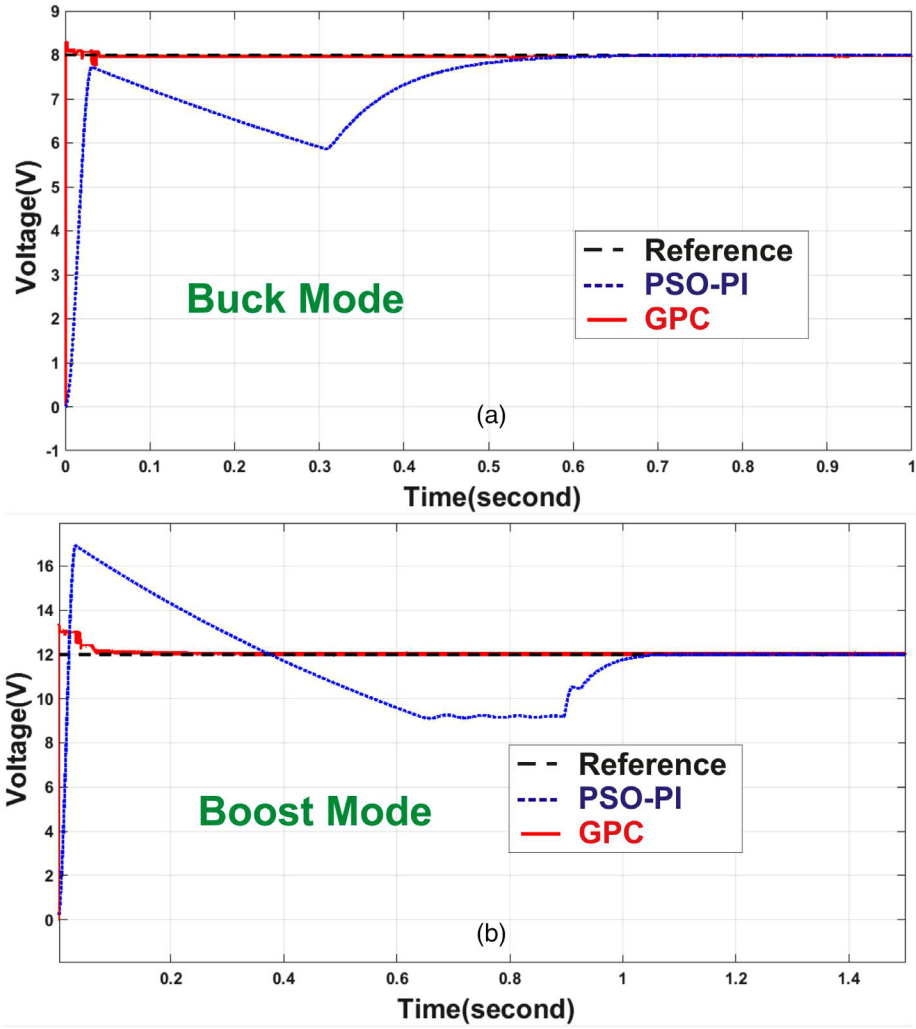


FIGURE 7 Buck-boost output voltage tracking with GPC and PID controllers ($R_{load} = 10 \Omega$)

TABLE 4 Detailed comparison based on Figure 6

Load	GPC-buck		PID-buck		GPC-boost		PID-boost	
	Overshoot	$t_{s,s}$	Overshoot	$t_{s,s}$	Overshoot	$t_{s,s}$	Overshoot	$t_{s,s}$
5Ω	0.22 V	0.04 s	—	0.41 s	0.22 V	0.035 s	1.85 V	1.05 s
8Ω	0.34 V	0.04 s	—	0.53 s	0.44 V	0.035 s	2.15 V	1.2 s
10Ω	0.37 V	0.04 s	—	0.56 s	0.54 V	0.035 s	2.3 V	1.4 s
12Ω	0.4 V	0.04 s	—	0.72 s	0.65 V	0.035 s	2.4 V	1.6 s

TABLE 5 Parameters of the PID controller

Parameters	Values
k_p	0.875
k_i	53.89
k_d	1.0038

TABLE 6 Performance comparison based on Figure 8

	GPC			PID		
	OS	US	Δ_t	OS	US	Δ_t
Ref changes	OS	US	Δ_t	OS	US	Δ_t
Negative step	—	—	0.5 s	—	—	—
Positive step	0.7 V	—	—	—	—	—

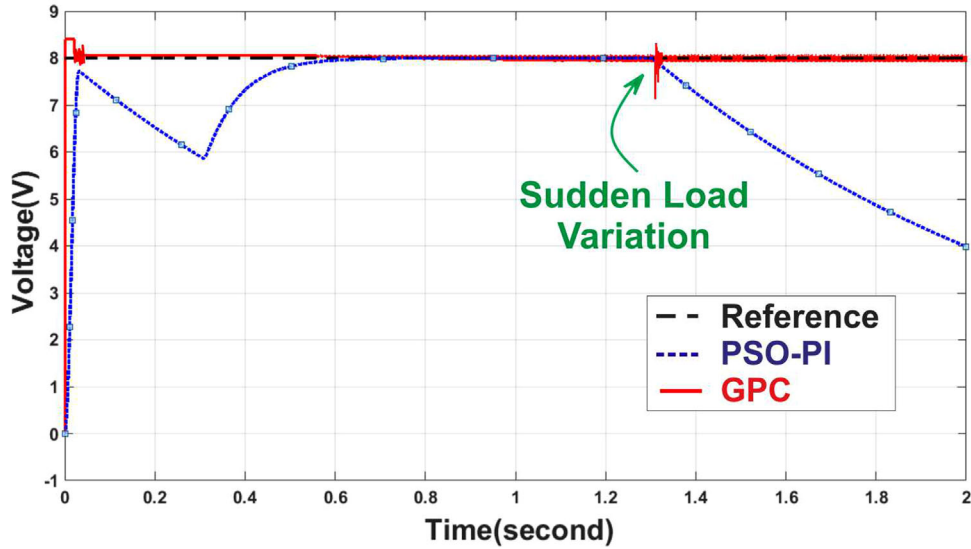


FIGURE 8 The impact of sudden load variation on control procedure of the controllers. ($R_{load} = 10 \Omega$ to $R_{load} = 30 \Omega$)

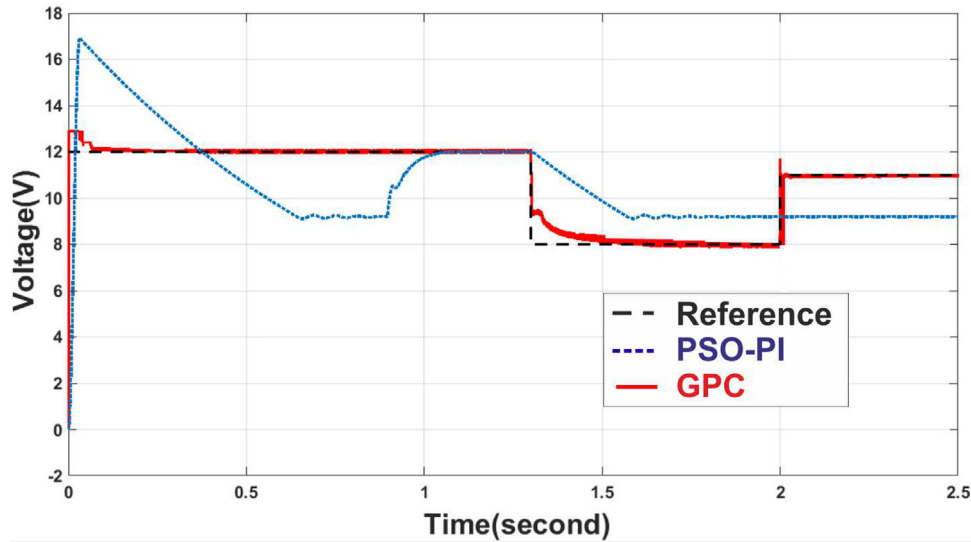


FIGURE 9 The tracking performance of the controllers in negative and positive reference alterations

Furthermore, the experimental results are examined for this converter to test the operation of the designed control method in experimental situations.

7 | EXPERIMENTAL RESULT

It should be noted that zero order hold (ZOH) technique is utilised to discrete the controller. Also, PWM scheme is used to fire the converter switches. To clarify this technique for better understanding, one can assume the PWM as a block that gets the control signal and compare it with a triangular signal, then a square wave is generated that has the role of actuating the switches. In Figure 12a hardware real-time implementa-

tion of converter is shown consisting of the power and control realisation, simultaneously.

Prototype machine shown in Figure 12 was implanted to analyse the accuracy of the GMPC for the topology. In addition, different segments and devices are included that are listed in Table 7. Arduino is the core of this structure which generates the control signal, while non-inverting DC–DC buck–boost converter is built based on the components listed in Table 3 with various loads to verify its performance under challenging dynamical variations.

Furthermore, the voltage sensor is attached to the load to transfer the output to the micro-processor to make the control signal by the aid of Matlab\Simulink ; also, the switching frequency is in the range of 20 KHz. The micro-processor

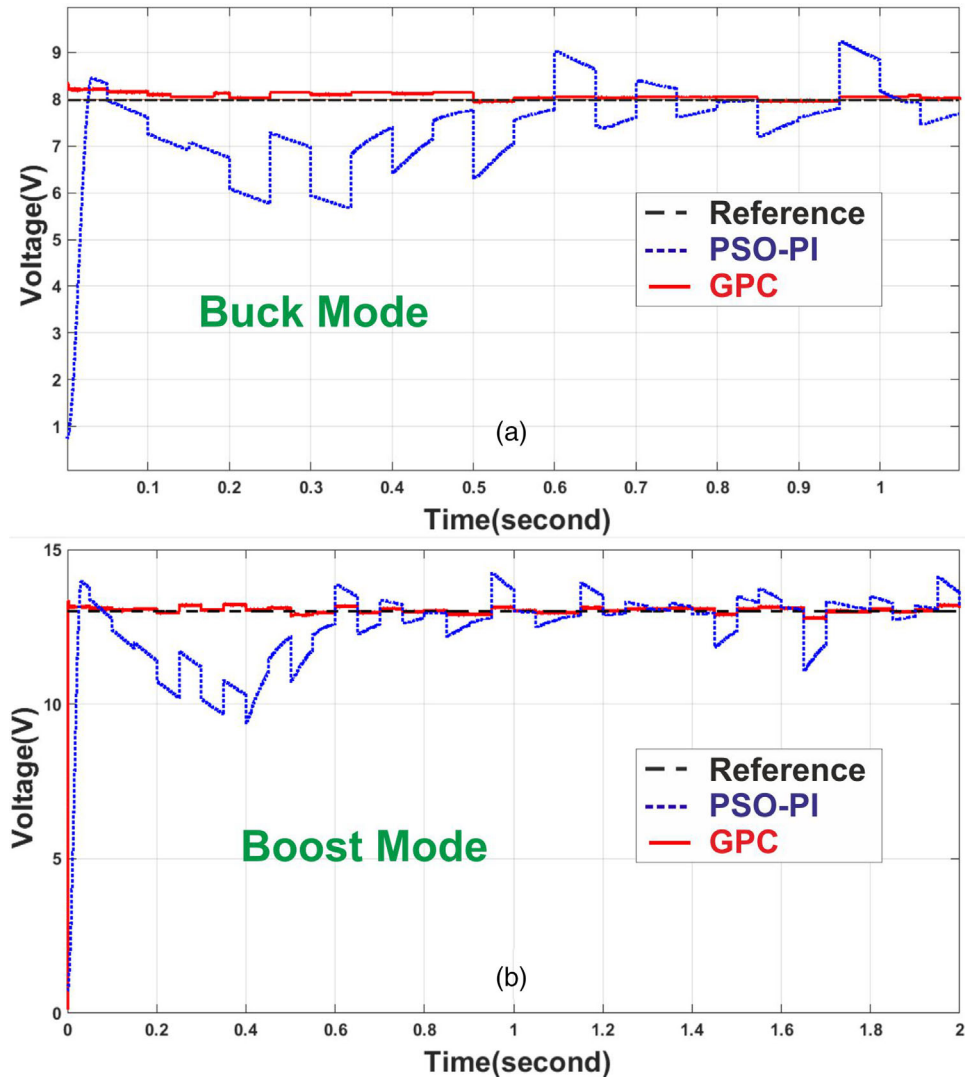


FIGURE 10 The performance of the proposed controllers in respond to noise; (a) noise with a variance of 0.01 in buck mode, (b) noise with a variance of 0.01 in boost mode

TABLE 7 Components of the structure

Components	Type
Micro-processor	Arduino (DUE)
Voltage sensor	LV25-P
Switches	IRF9630
Diodes	UF4007
IC gate driver MOSFET	TC4427

tries to convert the voltage measured by the sensor through its analogue-to-digital block, then the average value generated in this process will be used as the input of the control loop. Two different level of output voltages including 8 and 12 V are generated in Figures 13–15.

In this section, the converter is analysed in real-time situations using adaptive GMPC. Firstly, the operation of the control strategy is tested without considering effective disturbances.

Figure 13 shows convergence of GMPC by a novel on-line optimiser for the 8 and 12 V references which depicts an excellent practical operation with no undershoot or overshoot.

As a matter of fact, the industrial environments that the converters are used do not an ideal condition; thus, there is a high chance of parametric variations or output load changes.

To reaffirm high efficiency and robust dynamics of GMPC in real-time applications, different load types will be fed to the converter.

The load fed to the converter can have other structures rather than the pure resistive load used here. Figure 14 shows the response of the converter with the control technique in the connection with resistive–capacitive load and resistive–inductive load. Interestingly, from Figure 14, a change in the type of load has no negative impact on the tracking response of the control strategy.

At the next step, noises with 0.01 and 0.1 variances are injected to the system of the converter with different levels of

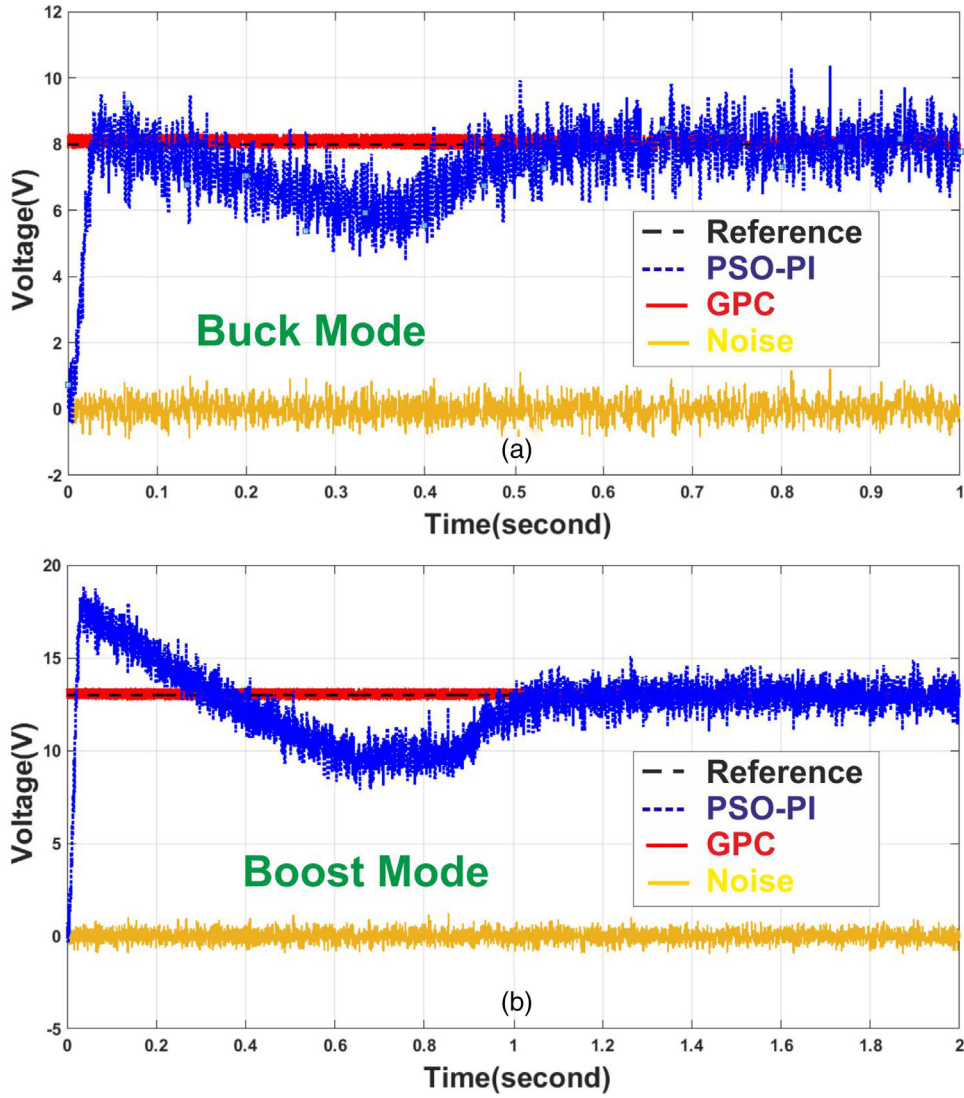


FIGURE 11 The performance of the proposed controllers in respond to noise; (a) 0.1 variance noise in buck mode, (b) 0.1 variance noise in boost mode

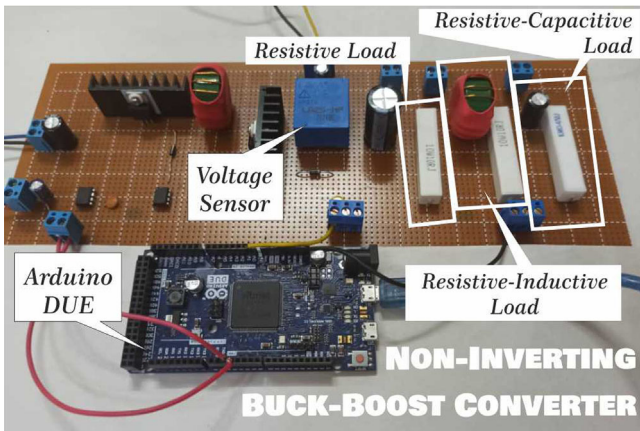


FIGURE 12 Topology of the non-inverting buck-boost converter in experimental environment

reference signal. The outcomes are shown for reference voltages of 8 and 12 V in Figures 15 and 16.

As it is vivid from Figures 15 and 16, by using the GMPC with IERLS identification method the effect of high variance noises on the converter can be compensated significantly that can propose it as a robust alternative for practical applications.

7.1 | Power efficiency

The total losses of the converter can be calculated by the proposed equation [46]:

$$P_{T-L} = P_{rL} + P_{rC} + P_{rT1} + P_{rT2} + P_{rQ1} + P_{rQ2} \quad (23)$$

where P_{rL} is inductor conduction loss, P_{rT1} and P_{rT2} are Diodes conduction loss, P_{rQ1} and P_{rQ2} are MOSFETs

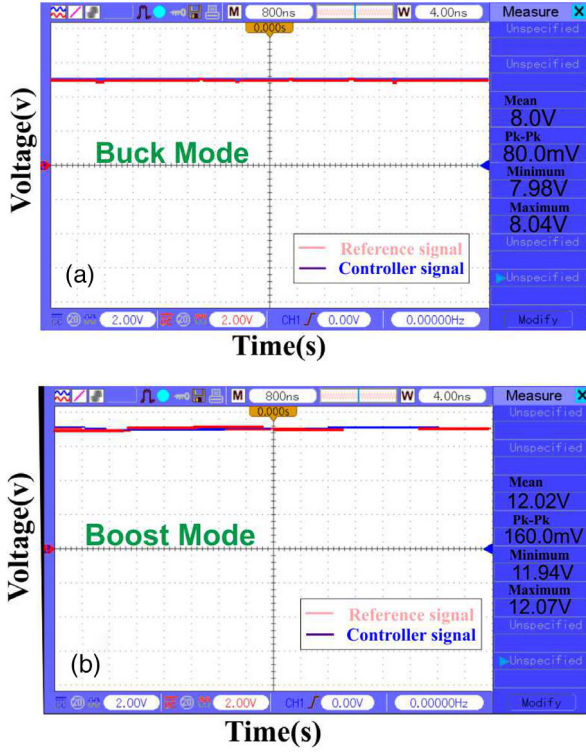


FIGURE 13 The GMPC with IERLS method on buck–boost converter. (a) tracking reference signal by controller in buck mode with reference of 8 DC voltage, (b) tracking reference signal by controller in boost mode with reference of 12 DC voltage

TABLE 8 The value of on-resistances on the components

Symbols	Values
r_L	5 m Ω
r_C	3 m Ω
r_{T1-2}	0.01 Ω
r_{Q1-2}	0.8 Ω

conduction loss, and P_{rC} is conduction loss of the capacitor [46]. To reach the losses presented in Equation (23), the calculations related to each loss is depicted in the following equations:

$$\begin{aligned}
 P_{rL} &= r_L \times I_L^2 \\
 P_{rC} &= r_C \times I_C^2 \\
 P_{rT1} &= r_{T1} \times I_{T1}^2 \\
 P_{rT2} &= r_{T2} \times I_{T2}^2 \\
 P_{rQ1} &= r_{Q1} \times I_{Q1}^2 \\
 P_{rQ2} &= r_{Q2} \times I_{Q2}^2
 \end{aligned} \tag{24}$$

In the above equation, the symbols of r_L and r_C are the resistances of inductor and capacitor; also, r_{T1-2} and r_{Q1-2} are the on-resistance of the diodes and the switches. The on-resistances related to these components are listed in Table 8.

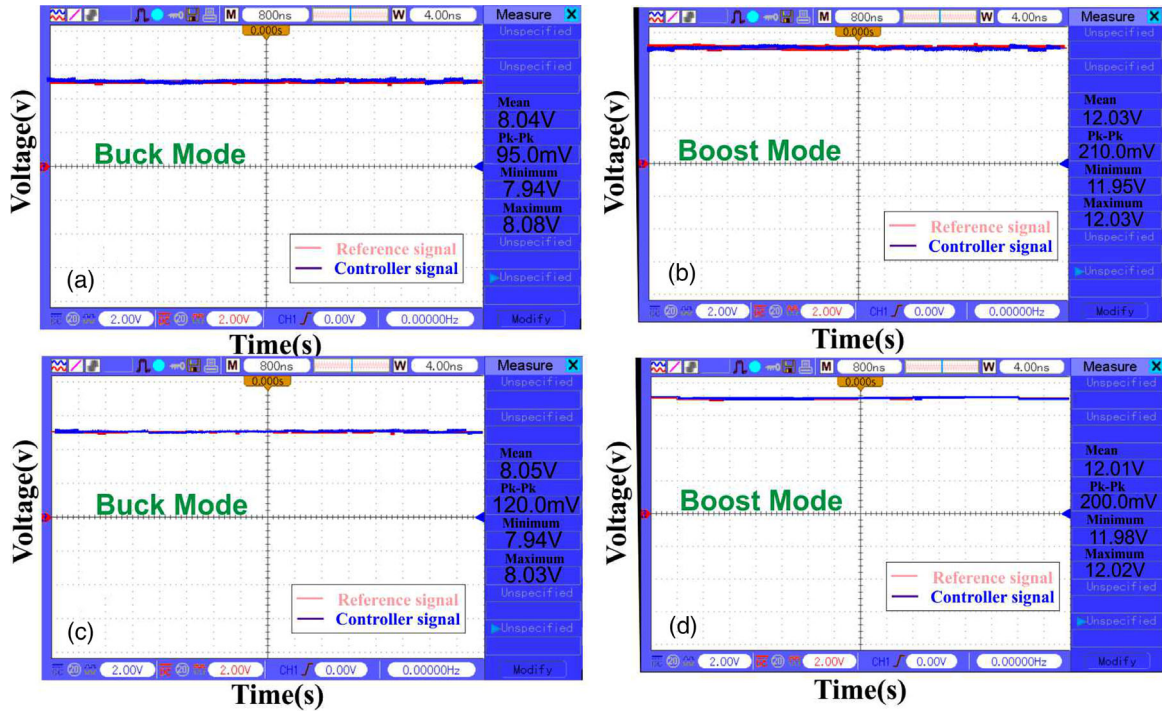


FIGURE 14 The performance of the adaptive GMPC method on buck–boost converter in the connection with different loads. (a) Tracking reference signal in resistive-inductive load in buck mode ($R = 30 \Omega, L = 1 \mu\text{H}$), (b) tracking reference signal in resistive-inductive load in boost mode ($R = 30 \Omega, L = 1 \mu\text{H}$), (c) tracking reference signal by controller in resistive-capacitive load in buck mode ($R = 50 \Omega, C = 10 \mu\text{F}$), (d) tracking reference signal by controller in resistive-capacitive load in boost mode ($R = 50 \Omega, C = 10 \mu\text{F}$)

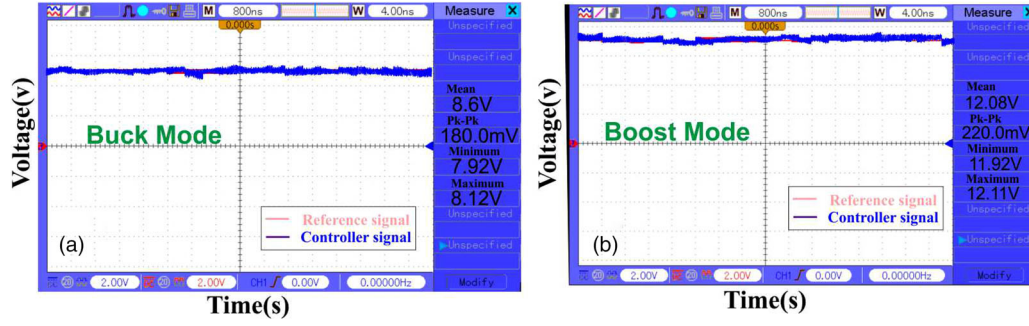


FIGURE 15 GPC controller on buck–boost converter with IERLS identification method by 0.01 variance noise for different tracking reference signals of; (a)8 V, (b)12 V

TABLE 9 The efficiency measured based on buck–boost converter

V_{out}	Measured efficiency (%)	Calculated efficiency (%)
15 V	94.56	98.12
20 V	93.42	96.27
25 V	92.47	94.53
30 V	90.63	92.34

Based on the output power of system (P_o), one can reach the total efficiency of the structure with the presented equation:

$$\eta = \frac{P_o}{P_o + P_{Total\ lossess}} \quad (25)$$

Considering the factors given in these equations, the level of efficiency of this structure is given in Table 9. It should be

TABLE 10 Comparison between the proposed controller and previous works. (Good=✓, very good=✓✓, high = +, very high=++)

Ref.	Control method	Dynamic complexity	Voltage tracking	Robustness in load disturbances	Optimisation	Robustness in noise	Maximum output power
[10]	SMC	+	✓	✓	Off-line	Not tested	27.8 W
[11]	SMC	++	✓	✓	Off-line	Not tested	33 W
[12]	IMC	++	✓✓	✓	Off-line	Not tested	22 W
[14]	IMC	+	✓	✓	Off-line	Not tested	7 W
[15]	DBC	+	✓	✓	Off-line	Not tested	35.2 W
[19]	FCS-MPC	++	✓✓	Not tested	Off-line	Not tested	3 kW
[22]	CCS-MPC	+	✓✓	✓	Off-line	Not tested	18.5 W
[24]	FCS-MPC	+	✓	✓	Off-line	Not tested	32.4 W
[26]	EMPC	++	✓✓	✓✓	Off-line	Not tested	18.8 W
[29]	NMPC	++	✓	Not tested	Off-line	Not tested	15 W
[30]	RMPC	++	✓✓	Not tested	Off-line	Not tested	14.5 W
[31]	PSO-MPC	+	✓✓	Not tested	Off-line	Not tested	24.5 W
[32]	NNMPC	+	✓✓	✓	On-line	Not tested	6.5 W
[33]	PSO-NNC	++	✓✓	✓✓	On-line	Not tested	120 W
[35]	STRAC	+	✓✓	✓✓	On-line	✓✓	20 W
[40]	PNNC	++	✓✓	✓	On-line	Not tested	28.4 W
[42]	CNAC	++	✓✓	✓	On-line	Not tested	22 W
[44]	MPC	++	✓✓	✓✓	On-line	Not tested	24 W
[47]	MPC	++	✓✓	✓	Off-line	Not tested	15.8 W
[48]	LM-MPC	++	✓✓	✓✓	Off-line	Not tested	22.6 W
[49]	MPC	+	✓	✓✓	Off-line	Not tested	194.6 W
[50]	NMPC	+	✓✓	✓	Off-line	Not tested	150 W
This work	GMPC	+	✓✓	✓✓	On-line	✓✓	180 W

noted that as the level of duty cycle increases, the total efficiency decreases, respectively.

8 | COMPARISON WITH PREVIOUS WORKS

To better clarify the merits of the designed GMPC, a detailed analyse is carried out in Table 10 based on different characteristics.

Considering the comparison illustrated in the above table, the efficiency of the presented work is higher in different working condition which can be introduced as an appropriate technique for industrial applications. In other words, the influence of noise is an inevitable phenomena in real-time applications which is not tested with almost none of the presented strategies but the proposed technique shows a great noise compensation result in both buck and boost modes. In addition, output generated power by this structure has a good practical level which can be used for supply of different loads and consumers.

9 | CONCLUSIONS

In this paper, GMPC with a novel IERLS identification method is applied on a non-inverting buck–boost DC–DC converter. The identification scheme considers the system as a black-box system that can decrease the computational burden of the controller. The GMPC uses an on-line optimisation structure based on IERLS that can improve the performance of the controller in harmful disturbance in both simulation and experimental environments. This discussed approach can maintain the stability margin in the desired limit under the presence of the parametric variations and large signal transients on the DC–DC converter. Additionally, both parts including the estimator and the GMPC are implemented by digital transfer function and have provided better performances against high variance noises and disturbing criterion. This predictive strategy shows much better responses in challenging conditions in comparison with other types of MPCs and conventional controllers as shown in Table 10. These results illustrate that by applying the adaptive GMPC, remarkable improvements occur in the performance of the converter over different operating conditions.

CONFLICT OF INTEREST

The authors declare no conflict of interest.

DATA AVAILABILITY STATEMENT

Data available on request from the authors

ORCID

Seyyed Morteza Ghamari  <https://orcid.org/0000-0001-5082-820X>

REFERENCES

- Lee, Y.S., Wang, S.J., Hui, S.Y.R.: Modeling, analysis, and application of buck converters in discontinuous-input-voltage mode operation. *IEEE Trans. Power Electron.* 12, 350–360 (1997)
- Hossain, M.Z., Rahim, N.A.: Recent progress and development on power DC–DC converter topology, control, design and applications: a review. *Renewable Sustainable Energy Rev.* 81, 205–230 (2018)
- Cheng, Y., Wen, G., Du, H.: Design of robust discretized sliding mode controller: analysis and application to Buck converters. *IEEE Trans. Ind. Electron.* 67, 10672–10681 (2020)
- Sira-Ramirez, Hebertt, J., Silva-Ortigoza, R.: *Control Design Techniques in Power Electronics Devices*, Springer, London (2006)
- Dragan, M.: Modeling and simulation of power electronic converters. *Proc. IEEE* 89, 898–912 (2001)
- Alma-aitah, M., Abuashour, M.I., Al-Hattab, M., et al.: Optimisation of PID controller employing PSO algorithm for interleaved buck–boost power electronic converter. *Int. J. Ind. Electron. Drives* 5, 49–55 (2019)
- Soh, J.H., Kang, S.W., Kim, R.Y.: Conduction loss analysis according to variation of resonant parameters in a zero-current switching boost converter. *J. Electr. Eng. Technol* 14, 2027–2037 (2019)
- Fishelov, A., Gazit, M., Radimov, N.: Digital average input current control in power converter. *U.S. Patent* 20,190,036,455, 10 Feb 1987
- Lu, Y., Ki, W.-H., Yue, C.P.: An NMOS-LDO regulated switched-capacitor DC–DC converter with fast-response adaptive-phase digital control. *IEEE Trans. Power Electron.* 31, 1294–1303 (2015)
- Taheri, B.: A new controller for DC–DC converters based on sliding mode control techniques. *J. Control, Autom. Electr. Syst.* 30, 63–74 (2019)
- Wang, B.: Deadbeat control for a single-inductor multiple-input multiple-output DC–DC converter. *IEEE Trans. Power Electron.* 34, 1914–1924 (2018)
- Cajamarca, B.: Sliding mode control based on internal model for a non-minimum phase buck and boost converter. *Enfoque UTE* 10, 41–53 (2019)
- Saadat, S., Amirhosein, A.: Adaptive neuro-fuzzy inference systems (ANFIS) controller design on single-phase full-bridge inverter with a cascade fractional-order PID voltage controller. *IET Power Electron.* 14, 1960–1972 (2021)
- Zhang, X.: Deadbeat control for single-inductor multiple-output DC–DC converter with effectively reduced cross regulation. *IEEE J. Emerg. Sel. Top. Power Electron.* 8(4), 3372–3381 (2019)
- Sarkar, S., Ghosh, S.S.: Comparison of different types of internal model controller architecture for a boost converter. In: *2020 IEEE International Conference on Power Electronics, Smart Grid and Renewable Energy (PESGRE2020)*, pp. 1–6. IEEE, Piscataway, NJ (2020)
- Borreggine, S.: A review on model predictive control and its applications in power electronics. In: *AEIT International Conference of Electrical and Electronic Technologies for Automotive*, pp. 1–6. IEEE, Piscataway, NJ (2019)
- Vazquez, S.: Model predictive control for power converters and drives: advances and trends. *IEEE Trans. Ind. Electron.* 64, 935–947 (2016)
- Bordons, C., Montero, C.: Basic principles of MPC for power converters: bridging the gap between theory and practice. *IEEE Ind. Electron. Mag.* 9, 31–43 (2015)
- Karamanakos, P.: Direct model predictive control: a review of strategies that achieve long prediction intervals for power electronics. *IEEE Ind. Electron. Mag.* 8, 32–43 (2014)
- Cheng, L.: Model predictive control for DC–DC boost converters with reduced prediction horizon and constant switching frequency. *IEEE Trans. Power Electron.* 33, 9064–9075 (2017)
- Cortés, P.: Guidelines for weighting factors design in model predictive control of power converters and drives. In: *IEEE International Conference on Industrial Technology*, pp. 1–7. IEEE, Piscataway, NJ (2009)
- Siami, M., Khaburi, D.A., Rodriguez, J.: Simplified finite control set-model predictive control for matrix converter-fed PMSM drives. *IEEE Trans. Power Electron.* 33, 2438–2446 (2017)
- Aguirre, M.: Switching frequency regulation for FCS-MPC based on a period control approach. *IEEE Trans. Ind. Electron.* 65, 5764–5773 (2017)

24. Cunha, R.B.A.: Constant switching frequency finite control set model predictive control applied to the boost converter of a photovoltaic system. *Solar Energy* 189, 57–66 (2019)
25. Luo, J.: A low voltage ride through strategy of DFIG based on explicit model predictive control. *Int. J. Electr. Power Energy Syst.* 119, 105783–105783 (2020)
26. Borreggine, S.: A review on model predictive control and its applications in power electronics. In: *AEIT International Conference of Electrical and Electronic Technologies for Automotive*, pp. 1–6. IEEE, Piscataway, NJ (2019)
27. Theunissen, J.: Regionless explicit model predictive control of active suspension systems with preview. *IEEE Trans. Ind. Electron.* 67, 4877–4888 (2019)
28. Shi, Y.: Design of explicit model predictive control for PMSM drive systems. In: *29th Chinese Control And Decision Conference (CCDC)*, p. 7389–7395. IEEE, Piscataway, NJ (2017)
29. Wang, Y.: Model predictive control strategy for energy optimization of seriesparallel hybrid electric vehicle. *J. Cleaner Prod.* 199, 348–358 (2018)
30. Lekić, A.: Microsecond nonlinear model predictive control for DC–DC converters. *Int. J. Circuit Theory Appl.* 48, 406–419 (2020)
31. Xie, Y.: Robust model predictive control based voltage regulation method for a distribution system with renewable energy sources and energy storage systems. *Int. J. Electr. Power Energy Syst.* 118, 105749–105749 (2020)
32. Velichko, A., Maksim B., Petr B.: A model of an oscillatory neural network with multilevel neurons for pattern recognition and computing. *Electronics*. 8(1) 75 (2019).
33. Saadatmand, S., Shamsi, P., Ferdowsi, M.: The voltage regulation of a buck converter using a neural network predictive controller. In: *2020 IEEE Texas Power and Energy Conference (TPEC)*, pp. 1–6. IEEE, Piscataway, NJ (2020)
34. Hamdi, H., Regaya, C.B., Zaafour, A.: Real-time study of a photovoltaic system with boost converter using the PSO-RBF neural network algorithms in a MyRio controller. *Solar Energy* 183, 1–16 (2019)
35. Ghamari, S.M., Mollae, H., Khavari, F.: Design of robust self-tuning regulator adaptive controller on single-phase full-bridge inverter. *IET Power Electron.* 13(16), 3613–3626 (2020)
36. Ghamari, S.M., Gholizadeh-Narm, H., Khavari, F.: Robust adaptive controller design for DC–DC SEPIC converter in photo voltaic application. In: *6th International Conference on Control, Instrumentation and Automation*, pp. 1–6. IEEE, Piscataway, NJ (2019)
37. Hasan, M.: A novel adaptive cascade controller design on a buck–boost DC–DC converter with a fractional-order PID voltage controller and a self-tuning regulator adaptive current controller. *IET Power Electron.* 14(11), 1920–1935 (2021)
38. Schaltz, E., Rasmussen, P.O., Khaligh, A.: Non-inverting buck–boost converter for fuel cell applications. In: *34th Annual Conference of IEEE Industrial Electronics*, pp. 855–860. IEEE, Piscataway, NJ (2008)
39. Govindharaj, A., Mariappan, A.: Real-time implementation of Chebyshev neural adaptive controller for boost converter. *Int. Trans. Electr. Energy Syst.* 30(6), 12394–12394 (2020)
40. Mohamed, A.A.: Predictive neural network based adaptive controller for gridconnected PV systems supplying pulse-load. *Solar Energy* 193, 139–147 (2019)
41. Basaran, K., Cetin, N.S.: Designing of a fuzzy controller for grid connected photovoltaic system's converter and comparing with PI controller. In: *IEEE International Conference on Renewable Energy Research and Applications (ICRERA)*, pp. 102–106. IEEE, Piscataway, NJ (2016)
42. Ghamari, S., Morteza, H., Mollae, F., et al.: Robust self-tuning regressive adaptive controller design for a DC–DC buck converter. *Measurement* 174, 109071–109071 (2021)
43. Ghamari, S., Morteza, Narm, H.H.G., et al.: Fractional-order fuzzy PID controller design on buck converter with antlion optimization algorithm. *IET Control Theory Appl.* 16, 340–352 (2022)
44. Güler, N., Irmak, E.: Design, implementation and model predictive based control of a mode-changeable DC/DC converter for hybrid renewable energy systems. *ISA Trans.* 114, 485–498 (2020)
45. Juneja, M., Nagar, S.K.: Particle swarm optimization algorithm and its parameters: a review. In: *2016 International Conference on Control, Computing, Communication and Materials (ICCCCM)*, pp. 1–6. IEEE, Piscataway, NJ (2016)
46. Özdemir, A., Erdem, Z.: Double-loop PI controller design of the DC–DC boost converter with a proposed approach for calculation of the controller parameters. *Proc. Inst. Mech. Eng., Part I: J. Syst. Control Eng.* 232(2), 137–148 (2018)
47. Aouni, E., Wassil, L.-A., Dessaint; Real-time implementation of input-state linearization and model predictive control for robust voltage regulation of a DC–DC boost converter. *IEEE Access* 8, 192101–192108 (2020)
48. Andrés-Martínez, O.: Nonlinear model predictive stabilization of DC–DC boost converters with constant power loads. *IEEE J. Emerg. Sel. Top. Power Electron.* 9, 822–830 (2020)
49. Güler, N., Irmak, E.: Design, implementation and model predictive based control of a mode-changeable DC/DC converter for hybrid renewable energy systems. *ISA Trans.* 114, 485–498 (2020)
50. Li, X., Liu, Y., Xue, Y.: Four-switch buck–boost converter based on model predictive control with smooth mode transition capability. *IEEE Trans. Ind. Electron.* 68(10), 9058–9069 (2020)

How to cite this article: Ghamari, S.M., Khavari, F., Mollae, H., Wheeler, P.: Generalised model predictive controller design for A DC–DC non-inverting buck–boost converter optimised with a novel identification technique. *IET Power Electron.* 1–15 (2022) <https://doi.org/10.1049/pel2.12309>